Structural Analysis and Theoretical Investigations of the Magnetocaloric Effect for La0.7Ba0.15Ag0.15MnO3 Manganite Prepared Using Sol-Gel Route

Sobhi Hcini, Mohamed Hsini, Hussein Al Robei, Mohamed Lamjed Bouazizi, Michel Boudard

Structural analysis and theoretical investigations of the magnetocaloric effect for La$_{0.7}$Ba$_{0.15}$Ag$_{0.15}$MnO$_3$ manganite prepared using sol-gel route

Sobhi Hcini [1,*]**, Mohamed Hsini** [2]**, Hussein Al Robei** [3]**, Mohamed Lamjed Bouazizi** [3]**, Michel Boudard** [4]

[1] *Research unit of valorization and optimization of exploitation of resources, Faculty of Science and Technology of Sidi Bouzid, Kairouan University, 9100 Sidi Bouzid, Tunisia.*
[2] *Laboratory of Physical Chemistry of Materials, Physics Department, Faculty of Sciences of Monastir, Monastir University, 5019 Monastir, Tunisia.*
[3] *Department of Mechanical Engineering, College of Engineering, Prince Sattam Bin Abdulaziz University, 11942 Alkharj, Saudi Arabia.*
[4] *University of Grenoble Alpes, LMGP, CNRS, 38000 Grenoble, France.*

* Corresponding author: E-mail address: hcini_sobhi@yahoo.fr (S. Hcini)

Abstract

Structural analysis, magnetocaloric properties, and theoretical investigations of the magnetocaloric effect were carried out in the crystalline La$_{0.7}$Ba$_{0.15}$Ag$_{0.15}$MnO$_3$ manganite prepared using sol-gel route. The phase purity and structure of this sample were checked by X-ray diffraction technique and Rietveld analysis. From magnetic measurements, the ferromagnetic to paramagnetic (FM-PM) phase transition was observed around T_C= 255 K. The maximum change in magnetic entropy (ΔS_M^{max}) and relative cooling power (RCP) extracted from magnetic measurements were 3.48 J×kg-1×K^{-1} and 225 J×kg^{-1} at an applied magnetic field of 5 T. These magnetocaloric parameters offer to the sample the possible use in the magnetic refrigeration technology. The magnetic-entropy simulation by using different theories such as the Weiss molecular mean-field theory and the Landau theory shows good correlation between the theoretical values of -$\Delta S_M(T)$ and the experimental ones estimated from Maxwell relation.

Keywords: Manganites; Sol-gel route, Structural analysis; Magnetocaloric effect; Spontaneous magnetization, Theoretical models.

1. Introduction

The magnetic refrigeration (MR) seems to be one of the very serious alternatives for replacing conventional refrigeration systems based on compression-expansion of gases [1]. This new technique, compared to the traditional techniques, has several advantages. It is more energy efficient, more compact and above all less harmful to the environment. The MR relies on the MCE (magnetocaloric effect), which is an intrinsic property of magnetic materials and results in an instantaneous and reversible variation of their temperature and entropy when they are subjected to a variation of magnetic field. This reversible effect is maximal at the FM-PM transition temperature (called the Curie temperature T_C), and is the consequence of the decrease in magnetic entropy following the alignment of the electronic spins under the application of the magnetic field. However, the optimization of the magnetic refrigerator devices depends on a solid thermodynamic description of the magnetic material. Different theories are developed and presented in this case. For example, the mean-field theory has established direct relations between magnetic entropy change and magnetization [2, 3]. Moreover, the theory of critical exponents justifies the existence of a universal magnetocaloric behavior in materials presenting second order magnetic phase transitions [4, 5]. The studies of critical exponents can supply valuable information about magnetic phase transitions. In addition, the Landau theory which is a mean field theory is used to the theoretical modeling of the MCE [6, 7]. The effect of the magnetoelastic coupling and electron condensation energy on the magnetic entropy change has been considered in this theory.

Among materials having good MCE, the manganites with perovskite structure adopting $Ln_{1-x}M_xMnO_3$ as general formula (Ln = trivalent rare earth element, and M = monovalent or divalent ion) represent a family of materials that was widely studied years ago for MR technology due to their rich properties [8-17]. Recently, these materials have been

widely studied due to their extremely high chemical stability over a wide range of compositions. This results in numerous modifications of their properties both on the fundamental scale and for potential applications.

In this work, we have prepared manganite sample with $La_{0.7}Ba_{0.15}Ag_{0.15}MnO_3$ composition using sol-gel method. This compound belongs to the family of lanthanum manganites and its silver-doped alloys, $La_{1-x}Ag_xMnO_3$, a subject of considerable renewed interest in the magnetic refrigeration technology [18-20]. We have successively studied the structural, and magnetocaloric properties for the $La_{0.7}Ba_{0.15}Ag_{0.15}MnO_3$ sample. We have also presented theoretical investigations of the magnetic entropy change for this sample using different theories, and the results were compared with the experimental ones.

2. Synthesis and characterizations

For the sol-gel synthesis of $La_{0.7}Ba_{0.15}Ag_{0.15}MnO_3$ manganite, the nitrates were selected as $La(NO_3)_3.6H_2O$, $Ba(NO_3)_2$, $AgNO_3$, and $Mn(NO_3)_34H_2O$, all with high purity. These nitrates were mixed according to the stoichiometric ratio and dissolved in distilled water with heating at 90 °C, followed by the addition of citric acid and ethylene glycol. Then, amounts of ammonia have been added in order to maintain the pH of the solution to about 7. After some time of heating (approximately 4 h), a viscous gel is observed. This gel was dried for 12 h at 250 °C, and the resulting precursor was ground in an agate mortar. The obtained powder was undergone two cycles of (grinding→ pelleting→ sintering) at 600 °C and 800 °C for 24 h, respectively. The resulting powder was sintered, in a final step, at 1000 °C for 24 h.

The phase purity of the synthesized sample was inspected via X-ray diffraction (XRD) technique, using Cu-Kα radiation (λ= 1.5406 Å). "*Fullprof*" program is used to perform the Rietveld refinement of structural parameters. "Quantum design" physical properties measurement system (PPMS) is used to measure both *M(T)* and *M(μ_0H, T)* data: *M(T)* curve was measured at ZFC (zero field cooling) at a weak magnetic field ($\mu_0H = 0.05$ T) in 150 K $\leq$

$T \leq 350$ K temperature range, and the $M(\mu_0 H, T)$ isotherm measurements were taken near T_C vs temperature in $0\ T \leq \mu_0 H \leq 5$ T magnetic field interval.

3. Results and discussions

3.1. XRD analysis

The XRD pattern for $La_{0.7}Ba_{0.15}Ag_{0.15}MnO_3$ manganite is shown in **Fig. 1a**. The pattern shows a pure perovskite phase with no detectable secondary phases. The sample crystallized in the rhombohedral crystal structure having space group $R\bar{3}c$ and space group number 167. The observed broadening of the diffraction peaks seems consistent with nanometric crystallite size. The structural parameters were calculated from Rietveld refinement of the obtained XRD pattern (**Fig. 1b**), and they are represented in **Table 1**. The obtained cell parameters are $a= b= 5.5216$ (1) Å, $c= 13.4259$ (3), $\alpha = 90$ °, $\beta = 90$ ° and $\gamma = 120$ °. The unit cell volume is $V= 354.487$ (8) $Å^3$. These lattice parameters are higher than those presented for the rhombohedral $La_{0.85}Ag_{0.15}MnO_3$ in Refs. **[21, 22]**. Obviously the Ba for La substitution causes the increase of lattice parameters in $La_{0.85}Ag_{0.15}MnO_3$ sample. This is in agreement with the smaller ionic radius of La ($r_{La}^{3+} = 1.032$ Å) compared to that for Ba ($r_{Ba}^{2+} = 1.35$ Å) **[23]**. The crystallite size was calculated using the full-width at half maximum (FWHM) of the most intense peak (1 1 0) by Scherrer's formula **[24]**:

$$t = \frac{0.9\,\lambda}{\beta \cos(\theta)} \tag{1}$$

where, β is the full width at half maximum of the peak at 2θ, θ is the corresponding Bragg angle, and λ is the wavelength. The measured crystallite size is about 46 nm. All the other structural parameters including site symmetry, Wyckoff positions, isotropic Debye-Waller factors, atomic positions, bond length, bond angle, and agreement factors are also presented in **Table 1**.

3.2. Magnetocaloric properties

Fig. 2a presents the $M(T)$ curve taken at $\mu_0H= 0.05$ T for $La_{0.7}Ba_{0.15}Ag_{0.15}MnO_3$ manganite. By representing the dM/dT curve (inset of **Fig. 2a**), the Curie temperature of the FM–PM phase transition was determined as $T_C = 255$ K. To understand the magnetic order in the sample, the magnetization $M(\mu_0H, T)$ isotherms are presented in **Fig. 2b**. As illustrated in this figure, the $M(\mu_0H, T)$ isotherms gradually decrease with increasing temperature. In addition, with the increase of μ_0H values, the magnetization increases non-linearly in the low temperature range with a tendency to saturation reflecting a ferromagnetic behavior, and varies linearly at high T values sign of paramagnetic behavior. **Fig. 2c**, shows the Arrott plots (M^2 vs μ_0H/M) which show positive slopes [25]. These positive slopes of M^2 vs μ_0H/M confirm the second-order magnetic phase-transition for $La_{0.7}Ba_{0.15}Ag_{0.15}MnO_3$ manganite [26]. The magnetic entropy $(-\Delta S_M)$ was given from $M(\mu_0H, T)$ data by the following Maxwell relations [1]:

$$\left(\frac{\partial S}{\partial \mu_0 H}\right)_T = \left(\frac{\partial M}{\partial T}\right)_{\mu_0 H} \tag{2}$$

$$\left(\frac{\partial S}{\partial M}\right)_T = -\left(\frac{\partial \mu_0 H}{\partial T}\right)_M \tag{3}$$

Using Eq. (2), the $-\Delta S_M$ values can be estimated as:

$$\Delta S_M(T, \Delta\mu_0 H) = \int_0^{\mu_0 H} \left(\frac{\partial M}{\partial T}\right)_{\mu_0 H} d\mu_0 H \tag{4}$$

The obtained $-\Delta S_M$ values for different applied fields are represented in **Fig. 2d**. As shown in this figure, the $-\Delta S_M(T)$ variation reaches a maximum peak near the order temperature (T_C) as $|\Delta S_M^{max}| = 3.48 J \times kg^{-1} \times K^{-1}$ at $\mu_0H= 5$ T. The relative cooling power (RCP) at different applied fields is estimated by multiplying the width at half height and the maximum value of magnetic entropy change according the following relation [1]:

$$RCP = |\Delta S_M^{max}| \times \delta T_{FWHM} \tag{5}$$

The RCP value is equal to 225 J kg^{-1} at $\mu_0 H = 5$ T. The RCP and $|\Delta S_M^{max}|$ values at $\mu_0 H = 5$ T for the present sample besides those of some Gd based materials [27], and other manganite samples [11-17] are compared in **Table 2**. We noted that the maximum entropy change for La$_{0.7}$Ba$_{0.15}$Ag$_{0.15}$MnO$_3$ sample, which is about 37 % of that of pure Gd, is larger than the $|\Delta S_M^{max}|$ values reported for some manganites considered for magnetic refrigeration technology [11, 13, 16], and much smaller than the pseudo binary alloy Gd$_5$Si$_2$Ge$_2$ [21]. However the sample exhibits a large relative cooling power which is about 55 % of that of Gd. Consequently, the present sample can be used as an active magnetic refrigerator in a relatively wide range of temperatures nearing 255 K with a relatively large entropy change.

3.3. Spontaneous magnetization

In the ferromagnetic state (below T_C), each ferromagnetic material acquires a spontaneous magnetization. The $(-\Delta S_M)$ expression is given *vs* the spontaneous magnetization (M_{spont}) as follows [28, 29]:

$$-\Delta S_M(\sigma) = \frac{3J}{J+1} N k_B \left(\sigma^2 + \sigma_{spont}^2\right) = \frac{3J}{M_0(J+1)} N k_B \left(M^2 + M_{spont}^2\right) \qquad (6)$$

where $\sigma_{spont} = \frac{M_{spont}}{M_0}$ is the reduced spontaneous magnetization, J is the angular spin value, N is the number of spins, k_B is the Boltzmann constant, and M_0 is the saturation magnetization. To estimate the spontaneous magnetization for La$_{0.7}$Ba$_{0.15}$Ag$_{0.15}$MnO$_3$ compound, we adjusted linearly the Arrott plots $\left(\frac{\mu_0 H}{M} \, vs \, M^2\right)$ in **Fig. 3a**, and the $(-\Delta S_M \, vs \, M^2)$ curves in **Fig. 3b** for $T < T_C$. These two figures show that all the curves obey the same regularity and have practically constant slopes in the temperature range below T_C. **Fig. 3c** shows a good agreement between M_{spont} values obtained according to the mean field theory and those calculated from Arrott plots. The good correlation between the both methods confirms the validity of the mean field theory for estimation of the spontaneous magnetization. According to the scaling method [30], the critical exponent (β) is associated to

M_{spont} and the reduced temperature $\varepsilon = \frac{T-T_C}{T_C}$ in the FM region $(T < T_C)$ by the following relation:

$$M_{spont} \approx log(M_0) + \beta log(-\varepsilon) \tag{7}$$

Using this relation, a linear adjustment of $log(M_{spont})$ vs $log(-\varepsilon)$ curve was carried out as shown in **Fig. 3d**. Here, we used the M_{spont} values estimated from $-\Delta S_M$ vs M^2 curves. The obtained β value ($\beta = 0.49$) is close to that of the mean field model ($\beta = 0.5$). This confirms the utility of the mean field theory in the case of our system.

3.4. Landau theory

According to the Landau's theory, the Gibbs free energy development to order six is given by [25]:

$$F(T,M) \cong F_0 + \frac{1}{2}A(T)M^2 + \frac{1}{4}B(T)M^4 + \frac{1}{6}C(T)M^6 + \cdots - MH, \tag{8}$$

here the Landau coefficients $A(T)$, $B(T)$, and $C(T)$ represent the magnetoelastic coupling and electrons interaction, and they are temperature-dependent parameters [31]. The examination of the free-energy expression demonstrates that the parameter $A(T)$ is always positive and would get a minimum value at the Curie temperature corresponding to a maximum of the susceptibility. On the other hand, the order of the magnetic transition is governed by the sign of $B(T)$ at the transition: a first-order transition takes place if $B(T) < 0$ while a second order occurs when $B(T) \geq 0$ [32]. Besides, $C(T)$ is positive at T_C but in other cases, it is negative or positive. By adjusting the Arrott curves (**Fig. 4a**), the three Landau coefficients are determined using the equation of the state given at the equilibrium condition $\left(\frac{dF(T,M)}{dM} = 0\right)$:

$$\frac{\mu_0 H}{M} = A(T) + B(T)M^4 + C(T)M^6. \tag{9}$$

Figs. 4(b-d) show the variations of A, B, and C coefficients vs T. From **Fig. 4c**, it is clear that $B(T)$ is positive at T_C confirming the second-order nature of the FM-PM transition. By deriving A, B and C vs T, the $-\Delta S_M(T)$ can be estimated as follows:

$$-\Delta S_M(T) = \frac{1}{2}A'M^2 + \frac{1}{4}B'M^4 + \frac{1}{6}C'M^6 \tag{10}$$

where $A' = \frac{\partial A}{\partial T}$, $B' = \frac{\partial B}{\partial T}$ and $C' = \frac{\partial C}{\partial T}$. **Fig. 5** shows a good agreement between $-\Delta S_M(T)$ curves obtained on the basis of Landau theory (red lines) and the experimental ones calculated using the Maxwell relation. Our results estimated by Landau theory, by pushing the development of the Gibbs function to order six, correlate better with the experimental ones than in the case of some other manganites **[33-36]** where the development of the Gibbs free energy was limited to order four.

3.5. Mean-field approach

The magnetization (*M*), for a ferromagnetic material, can be adjusted according to the Brillouin function $B_J(x)$ as **[37]**:

$$M = f\left(\frac{\mu_0 H + H_{exch}}{T}\right) = M_0 B_J(x) \tag{11}$$

where *T* is the temperature, $\mu_0 H$ is the applied magnetic field, $H_{exch} = \lambda M$ is the exchange field (λ is the mean-field exchange parameter), and $B_J(x)$ function can be expressed as:

$$B_J(x) = \frac{2J+1}{2J}\coth\left(\frac{2J+1}{2J}x\right) - \frac{1}{2J}\coth\left(\frac{x}{2J}\right) \text{ with } x = \frac{Jg\mu_B}{k_B}\left(\frac{\mu_0 H + H_{exch}}{T}\right) \tag{12}$$

with *J*= spin momentum, *g*= gyromagnetic factor, μ_B= Bohr magneton, k_B= Boltzmann constant. By applying the reciprocal function of f on the first member of Eq. (11), we can obtain:

$$\frac{\mu_0 H}{T} = f^{-1}(M) - \frac{H_{exch}}{T} = f^{-1}(M) - \frac{\lambda M}{T}. \tag{13}$$

Using **Fig 2b**, we plotted in **Fig 6a** the variation of $\mu_0 H/T$ vs. *1/T* at constant *M* step (5 $Am^2 \times kg^{-1}$). It's clear that the obtained iso-magnetization curves have a linear trend. Linear adjustments are then made on the linear parts of the iso-magnetization curves (red solid lines) giving the H_{exch} values. In **Fig. 6b** we present the H_{exch} *vs M* curve which has been adjusted using the following relation **[38, 39]**:

$$H_{exch} = \lambda_1 M + \lambda_3 M^3 \tag{14}$$

The adjustment shows negligible value of λ_3 parameter ($\lambda_3 = -0.0001$ (T $\times$ Am^{-2} $\times$ kg)^3), so the H_{exch} expression can be approximated as $H_{exch} = \lambda M$, with $\lambda = \lambda_1 = 1.098$ T $\times$ Am^{-2} $\times$ kg.

The next step of this theory is to construct the M vs $\left(\frac{\mu_0 H + H_{exch}}{T}\right)$ curves which are shown in **Fig. 7** (black symbols). As observed, all these curves overlap in a single curve which has been adjusted using the Brillouin function as illustrated in Eq. (11). This adjustment represented by red line in **Fig. 7** allows finding the values of *J*, *g* and *M$_0$* respectively as 2.03, 2.04 and 65 Am^2×kg^{-1}. These values can be compared with the theoretical ones. In this case, the theoretical values of *J* and *g* are estimated by respecting the Hund rules **[40]**. As the orbital moment (*L*) is blocked for the transition metal ions **[40]**, only the contributions of Mn^{3+} and Mn^{4+} are considered for $La_{0.7}^{3+}Ba_{0.15}^{2+}Ag_{0.15}^{2+}Mn_{0.55}^{3+}Mn_{0.45}^{4+}O_3^{2-}$ sample, giving $J = g =2$. It is clear that the experimental values of *J* and *g* match well with the theoretical ones. Thereafter, the adjusted values of *M$_0$*, *J* and *g* were injected into Eq. (11) in order to generate the theoretical $M(\mu_0 H, T)$ isotherms represented by solid red lines in **Fig. 8a** which correlate well with the experimental isotherms indicated by black symbols. This confirms the utility of the mean field approach in the present study. On another side, according to the Bean-Rodbell model, the reduced magnetization (σ) is expressed as a function of the Brillouin function as **[41, 42]**:

$$\sigma(Y) = B_J(Y), \tag{15}$$

With

$$Y = \frac{1}{T}\left[3T_0\left(\frac{J}{J+1}\right)\sigma + \frac{gJ\mu_B}{k_B}\mu_0 H + \frac{9}{5}\frac{(2J+1)^4-1}{[2(J+1)]^4}T_0\eta\sigma^3\right] \tag{16}$$

where *T$_0$* is the transition temperature, and η is a parameter which can also checks the phase-transition order. Indeed, if $\eta < 1$ a second order transition takes place; however a first order transition appears when $\eta > 1$. Then, to model *M vs T* under different magnetic field by the

Bean-Rodbell model, we replace x in Eq. (11), by Y in Eq. (16). A simulation of the experimental $M(T)$ curves is established for $\eta = 0.07$ and $T_0 = 255$ K (see **Fig. 8b**). Seeing that $\eta < 1$, the present sample presents a FM-PM phase transition of second-order type. The simulation of the curves of $-\Delta S_M(T)$ is achieved using the following relation:

$$-\Delta S_M(T)_{H_1 \rightarrow H_2} = \int_{M|_{H_1}}^{M|_{H_2}} \left(f^{-1}(M) - \left(\frac{\partial \lambda(T)}{\partial T} \right)_M M \right) dM \qquad (17)$$

Fig. 9 presents a comparison between the simulated $-\Delta S_M(T)$ curves (red lines) obtained using the mean field theory combined with the Bean-Rodbell model, and the experimental ones deduced from the Maxwell relation (black symbols). This simulation of the magnetic entropy variation shows well correlation between the simulated curves and the experimental ones. These results are in good agreement with those presented in previous works **[28, 31, 38, 39]**, where the mean field theory combined with the Bean-Rodbell model was used to estimate the magnetic entropy change from the data on the temperature and field dependences of the magnetization.

4. Conclusion

In this work the $La_{0.7}Ba_{0.15}Ag_{0.15}MnO_3$ manganite sample was prepared by sol-gel route. XRD analysis shows that the compound is good crystallized and its majority phase is a perovskite with rhombohedral $R\overline{3}c$ structure. The $M(T)$ measurement shows a second order FM-PM phase transition at $T_C = 255$ K. From an application perspective, the sample can be used in the MR technology. An analysis of the spontaneous magnetization, $M_{spont}(T)$, was also carried out using the ($-\Delta S_M$ vs M^2) and ($\mu_0 H/M$ vs M^2) data. The molecular mean-field, Bean Rodbell and Landau theories, were developed to model the magnetic entropy change for the sample. The theoretical results show good agreement with the experimental ones.

Acknowledgments

References

[1] M.H. Phan, S.C. Yu, J. Magn. Magn. Mater. 308 (2007) 325.

[2] M. Hsini, S. Khadhraoui, N. Zaidi, Z.A. Alrowaili, J. Supercond. Nov. Magn. 31 (2018) 3717.

[3] S. Khadhraoui, M. Baazaoui, M. Hsini, M. Oumezzine, J. Supercond. Nov. Magn. 32 (2019) 291.

[4] V. Franco, A. Conde, E.J.M. Romero, J.S. Blazquez, J. Phys. Condens. Matter 20 (2008) 285207.

[5] S. Hcini, M. Boudard, S. Zemni, M. Oumezzine, Ceram. Int. 41 (2015) 2042.

[6] E. Oumezzine, M. Oumezzine, E.K. Hlil, J. Alloys Compd. 682 (2016) 366.

[7] S. Kallel, N. Kallel, O. Pe~na, M. Oumezzine, Mater. Lett. 64 (2010) 1045.

[8] H. Yang, Q. Wu, N. Yu, Y. Yu, M. Pan, P. Zhang, H. Ge, J. Solid State Chem. 282 (2020) 121072.

[9] A.O. Ayaş, S.K. Çetin, M. Akyol, G. Akça, A. Ekicibil, J. Mol. Struct. 1200 (2020) 127120.

[10] A.D. Souza, M.S. Murari, M.D. Daivajna, Physica B Condens Matter. 580 (2020) 411909.

[11] E. Oumezzine, S. Hcini, E.K. Hlil, E. Dhahri, M. Oumezzine, J. Alloys Compd. 615 (2014) 553.

[12] S. Hcini, M. Boudard, S. Zemni, M. Oumezzine, Ceram. Int. 40 (2014) 16041.

[13] M. Baazaoui, M. Boudard, S. Zemni, Mater. Lett. 65 (2011) 2093.

[14] D.N.H. Nam, N.V. Dai, L.V. Hong, N.X. Phuc, S.C. Yu, M. Tachibana, E. Takayama-Muromachi, J. Appl. Phys. 103 (2008) 043905.

[15] S. Mahjoub, M. Baazaoui, E.K. Hlil, M. Oumezzine, Ceram. Int. 41 (2015) 12407.

[16] C.P. Reshmi, S.S. Pillai, K.G. Suresh, M.R. Varma, Solid State Sci. 19 (2013) 130.

[17] Y. Sun, W. Tong, Y.H. Zhang, J. Magn. Magn. Mater. 232 (2001) 205.

[18] T. Tang, K.M. Gu, Q.Q. Cao, D.H. Wang, S.Y. Wang, S.Y. Zhang, Y.W. Du, J. Magn. Magn. Mater. 222 (2000) 110.

[19] N.T. Hien, N.P. Thuy, Physica B Condens Matter. 319 (2002) 168.

[20] A.G. Gamzatov, A.S. Mankevich, Bull. Lebedev Phys. Inst. 36 (2009) 367.

[21] A.O. Ayaş, M. Akyol, A. Ekicibil, Philos. Mag. 96 (2016) 922.

[22] C.B. Larsena, S. Samothrakitis, A.D. Fortes, A.O. Ayaş, M. Akyol, A. Ekicibil, M. Laver, J. Magn. Magn. Mater. 498 (2020) 166192.

[23] R.D. Shannon, Acta Cryst. A 32 (1976) 751.

[24] S. Hcini, S. Zemni, A. Triki, H. Rahmouni, M. Boudard, J. Alloys Compd. 509 (2011) 1394.

[25] A. Arrott, Phys. Rev. 108 (1957) 1394.

[26] S.K. Banerjee, Phys. Lett. 12 (1964) 16.

[27] V.K. Pecharsky Jr., K.A. Gschneidner, J. Magn. Magn. Mater. 167 (1997) L179.

[28] S. Khadhraoui, N. Zaidi, M. Hsini, Z.A. Alrowaili, J. Supercond. Nov. Magn. 32 (2019) 1285.

[29] G.J. Liu, J.R. Sun, J. Lin, Y.W. Xie, T.Y. Zhao, H.W. Zhang, B.G. Shen, Appl. Phys. Lett. 88 (2006) 212505.

[30] H.E. Stanley, Introduction to Phase Transitions and Critical Phenomena, Oxford University Press, London, 1971.

[31] M. Hsini, S. Hcini, S. Zemni, J. Supercond. Nov. Magn. 31 (2018) 81.

[32] V.S. Amaral, J.S. Amaral, J. Magn. Magn. Mater. 272–276 (2004) 2104.

[33] S. Das, T.K. Dey, J. Phys. Condens. Matter. 18 (2006) 7629.

[34] S. Das, T.K. Dey, J. Alloys Comp. 440 (2007) 30.

[35] S. Das, T.K. Dey, J. Phys D, Appl Phys 40 (2007) 1855.

[36] S. Das, T.K. Dey, Mat. Chem. Phys. 108 (2008) 220.

[37] L. Jia, J. Sun, H. Zhang, F. Hu, C. Dong, B. Shen, J. Phys. Condens. Matter. 18 (2006) 9999.

[38] S. Yahyaoui, M. Khalfaoui, S. Kallel, N. Kallel, J.S. Amaral, A. Ben Lamine, J. Alloys Compd. 685 (2016) 633.

[39] S. Yahyaoui, M. Khalfaoui, S. Kallel, N. Kallel, J.S. Amaral, A. Ben, Lamine, J. Magn. Magn. Mater. 393 (2015) 105.

[40] C. Kittel, Introduction to Solid State Physics, 7th edn. (Wiley, New York, 1996).

[41] A.M. Tishin, Y.I. Spichkin, The Magnetocaloric Effect and its Applications, IOP Publishing, London, 2003.

[42] R. Zach , M. Guillot, J. Tobola, J. Appl. Phys. 83 (1998) 7237.

Table legends

Table 1: Rietveld refinement of the structural parameters for $La_{0.7}Ba_{0.15}Ag_{0.15}MnO_3$ manganite. The numbers in parentheses are estimated standard deviations to the last significant digit.

Sample				$La_{0.7}Ba_{0.15}Ag_{0.15}MnO_3$
Cell parameters	*a (Å)*			5.5216 (1)
	c (Å)			13.4259 (3)
	V (Å³)			354.487 (1)
Atoms	*La/Ba/Ag*	*Wyckoff Positions*		6a
		Site Symmetry		32
		Atomic Positions	*(x, y, z)*	(0, 0, ¼)
		Isotropic Debye-Waller factor	B_{iso} *(Å²)*	1.18 (3)
	Mn	*Wyckoff Positions*		6b
		Site Symmetry		-3
		Atomic Positions	*(x, y, z)*	(0, 0, 0)
		Isotropic Debye-Waller factor	B_{iso} *(Å²)*	0.20 (0)
	O	*Wyckoff Positions*		18e
		Site Symmetry		2
		Atomic Positions	*(x, y, z)*	(0.5201 (2), 0, ¼)
		Isotropic Debye-Waller factor	B_{iso} *(Å²)*	2.04 (1)
Structural parameters		*Bond length*	d_{Mn-O} *(Å)*	1.9505 (6)
		Bond angle	$\theta_{Mn-O-Mn}$ *(°)*	173.51 (3)
		Average grains size	*t (nm)*	46
Agreement factors	*Profile factor*		R_p *(%)*	1.43
	Weighted profile factor		R_{wp} *(%)*	2.01
	Structure factor		R_F*(%)*	3.15
	Goodness of fit		χ^2 *(%)*	2.53

Table 2: Magnetocaloric parameters at $\mu_0 H = 5$ T for $La_{0.7}Ba_{0.15}Ag_{0.15}MnO_3$ manganite (present work) compared to several materials considered for magnetic refrigeration technology.

| Samples	T_C (K)	$\Delta\mu_0 H$ (T)	$|\Delta S_M^{max}|$ (J×Kg^{-1}×K^{-1})	RCP (J×Kg^{-1})	Ref.
$La_{0.7}Ba_{0.15}Ag_{0.15}MnO_3$	255	5	3.48	225	Present work
Gd	293	5	9.5	410	[21]
$Gd_5Si_2Ge_2$	275	5	18.5	535	[21]
$La_{0.6}Pr_{0.1}Ba_{0.3}MnO_3$	215	5	1.97	230	[5]
$La_{0.6}Pr_{0.1}Ba_{0.3}Mn_{0.9}Ni_{0.1}O_3$	162	5	1.31	123	[5]
$Nd_{0.67}Ba_{0.33}MnO_3$	145	5	3.91	265	[6]
$Nd_{0.67}Ba_{0.33}Mn_{0.98}Fe_{0.02}O_3$	134	5	2.97	242	[6]
$La_{0.67}Ba_{0.33}Mn_{0.95}Fe_{0.05}O_3$	271	5	2.54	246	[7]
$Pr_{0.67}Ba_{0.33}Mn_{0.95}Fe_{0.05}O_3$	128	5	3.09	287	[7]
$La_{0.7}Sr_{0.3}Mn_{0.95}Al_{0.05}O_3$	332	5	4.4	-	[8]
$Pr_{0.6}Ca_{0.1}Sr_{0.3}Mn_{0.975}Fe_{0.025}O_3$	235	5	3.53	192	[9]
$La_{0.67}Sr_{0.33}Mn_{0.9}Ni_{0.1}O_3$	290	5	3	132	[10]
$La_{0.67}Sr_{0.33}Mn_{0.9}Co_{0.1}O_3$	328	5	5.00	200	[11]
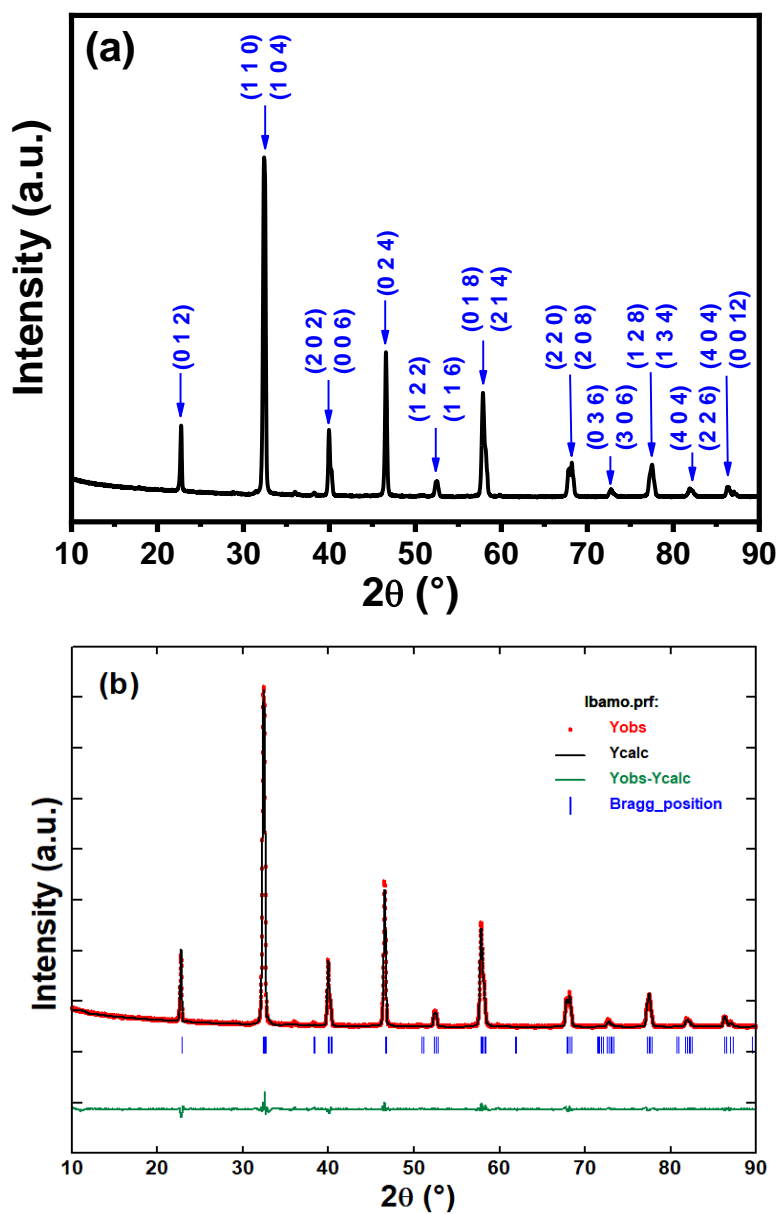
Fig. 1: (a) X-ray diffraction pattern for $La_{0.7}Ba_{0.15}Ag_{0.15}MnO_3$ manganite. All peaks are indexed in the hexagonal setting of the rhombohedral $R\overline{3}c$ symmetry. **(b)** Rietveld analysis of XRD pattern. The bottom line (green) represents the difference between the XRD data (red) and calculated fit (black), and the blue lines are Bragg positions.
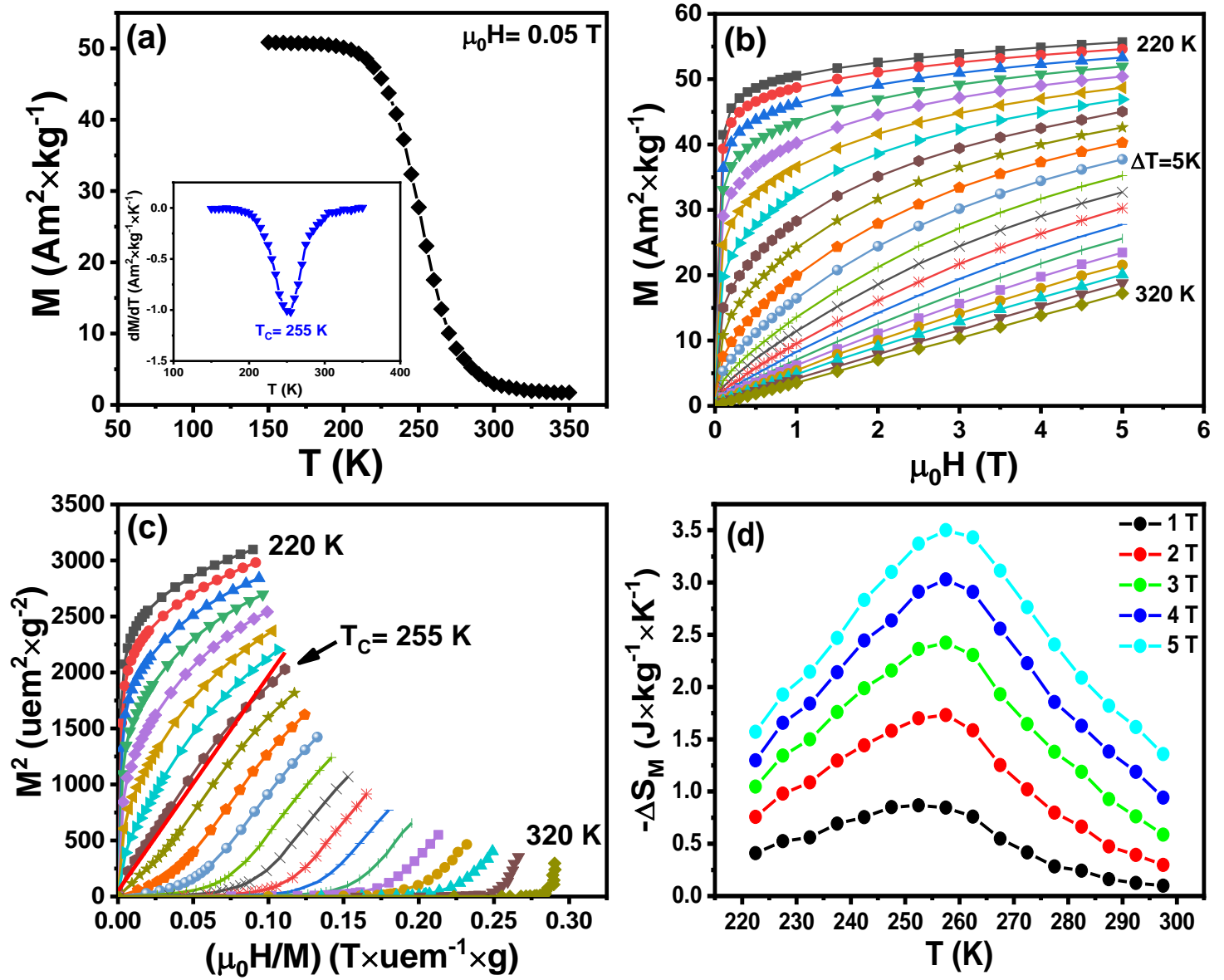
Fig. 2: (a) Temperature dependence of magnetization and *dM/dT vs T* curve at μ_0H= 0.05 T. **(b)** Magnetization isotherms. **(c)** Arrott plots around T_C. **(d)** Magnetic entropy change *vs T* at various applied magnetic fields.
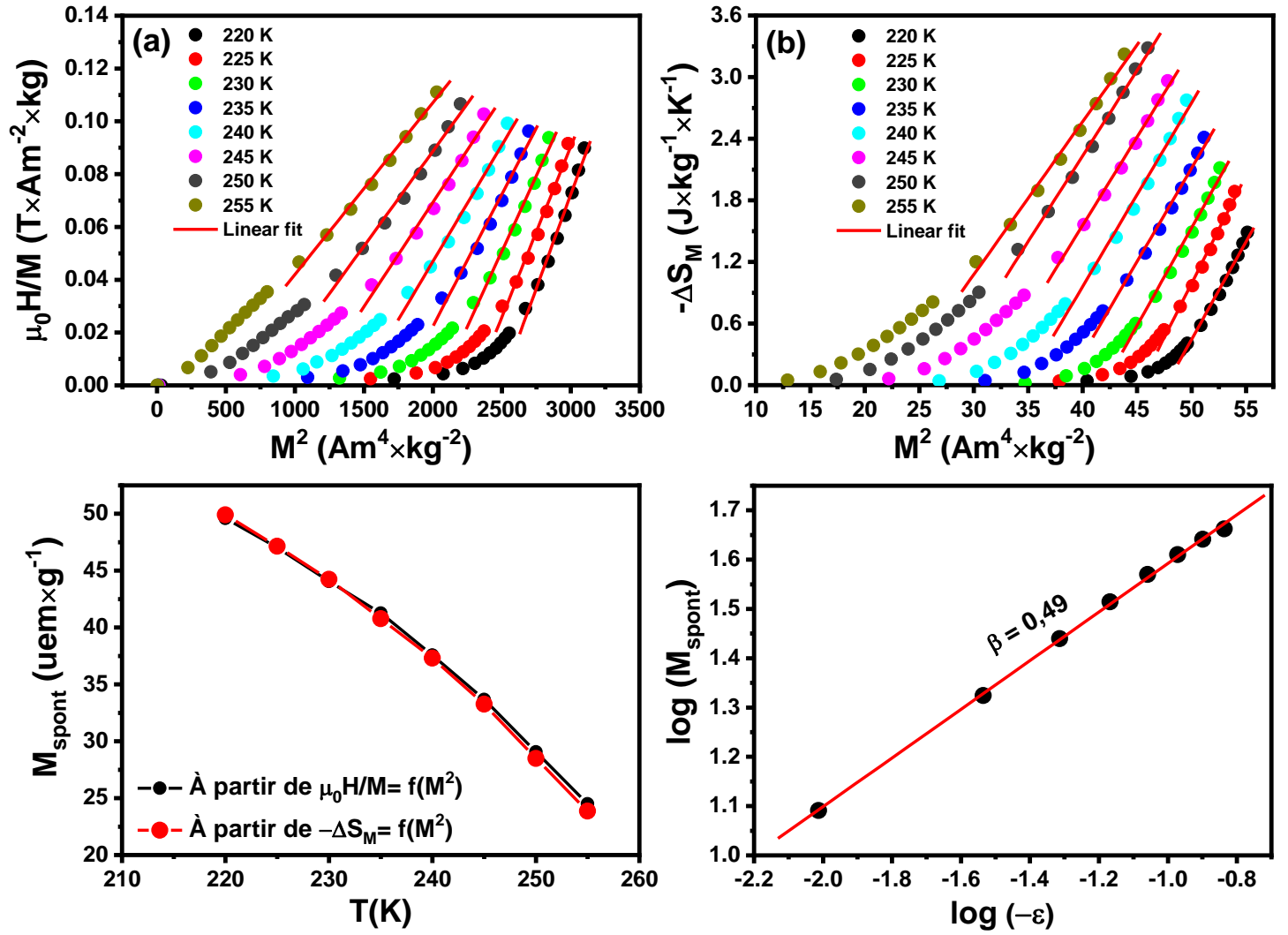
Fig. 3: (a) Linear fits (red lines) for $T < T_C$ of Arrott plots $\left(\frac{\mu_0 H}{M}\ vs\ M^2\right)$. **(b)** Linear fits (red lines) of $-\Delta S_M\ vs\ M^2$ curves. **(c)** M_{spont} vs T deduced from $-\Delta S_M\ vs\ M^2$ curves *(black symbols)* and from the Arrott plots $\left(\frac{\mu_0 H}{M}\ vs\ M^2\right)$ *(red symbols)*. **(d)** Linear fit of $log\ M_{spont}\ vs\ log\ (-\varepsilon)$ deduced from $-\Delta S_M\ vs\ M^2$ curves.
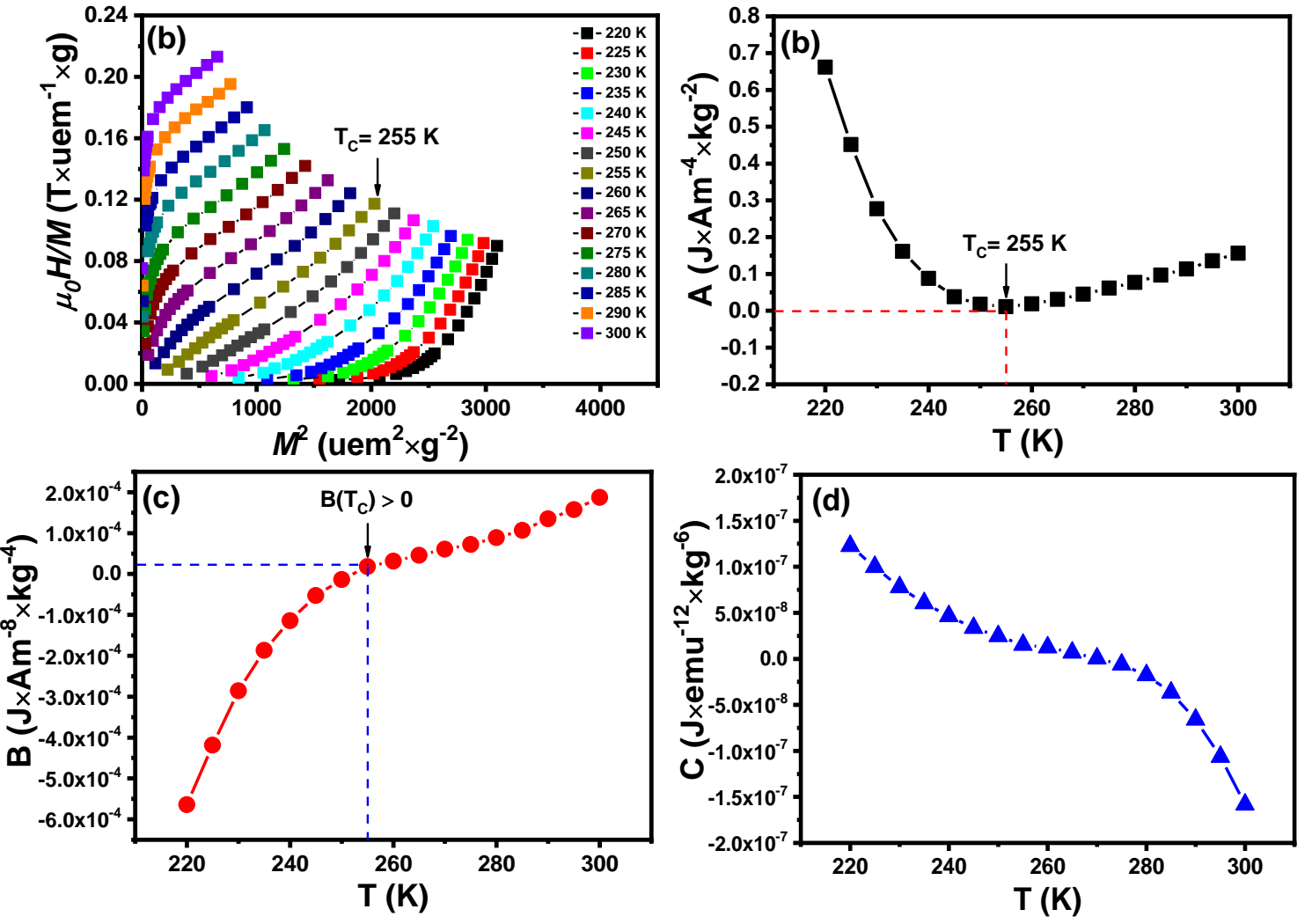
Fig. 4: (a) Quadratic fit (red lines) of $\left(\frac{\mu_0 H}{M} \ vs \ M^2\right)$. **(b)** Variation of Landau parameter *A(T)*. (**c**) Variation of Landau parameter *B(T)*. (**d**) Variation of Landau parameter *C(T)*.
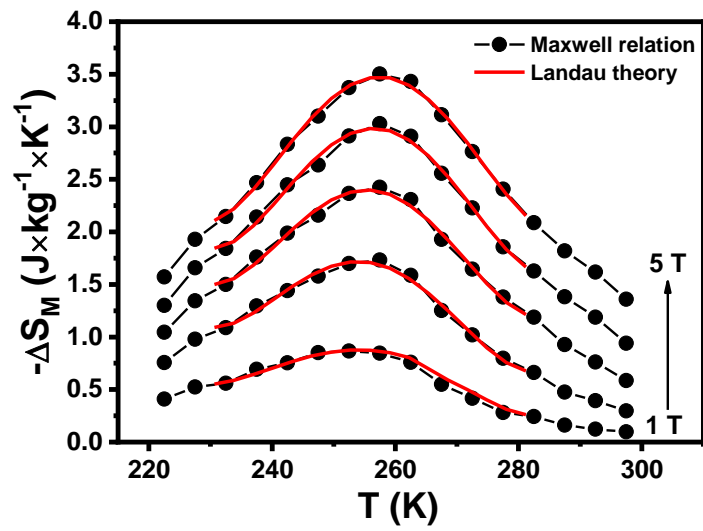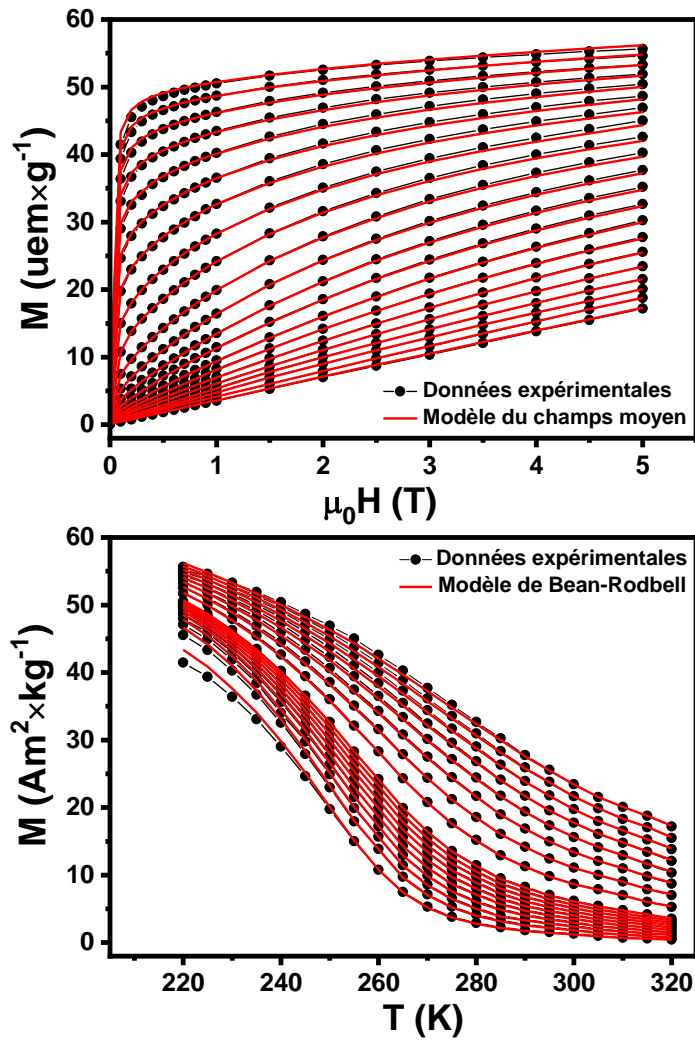
Fig. 5: Comparison between $-\Delta S_M$ *vs T* under various applied magnetic fields estimated from Maxwell relation (black symbols) and Landau theory (red lines).
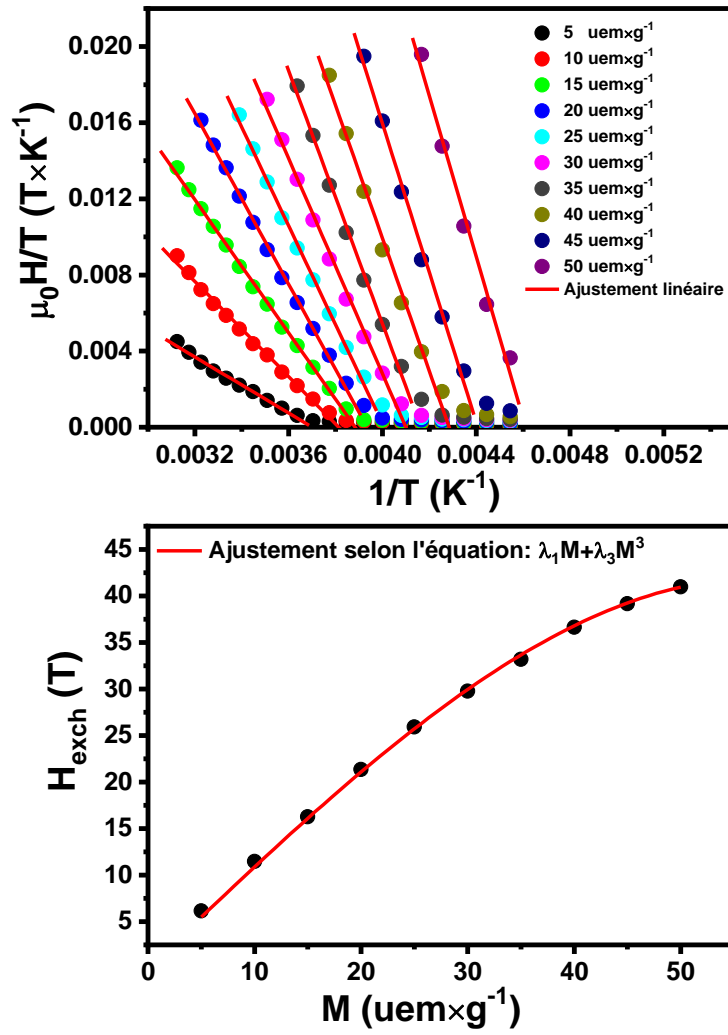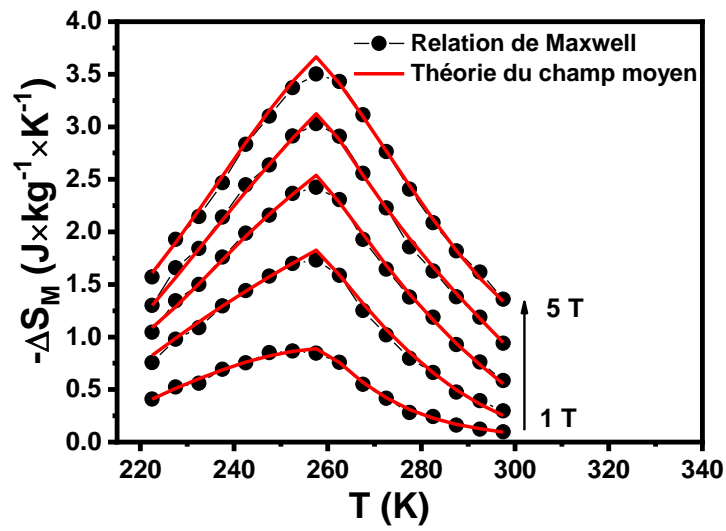
Fig. 6: **(a)** $\frac{\mu_0 H}{T}$ *vs* $\frac{1}{T}$ curves under constant magnetization ($M = 5 \text{ Am}^2 \times \text{kg}^{-1}$). **(b)** H_{exch} *vs* M fitted by $\lambda_1 M + \lambda_3 M^3$ function.
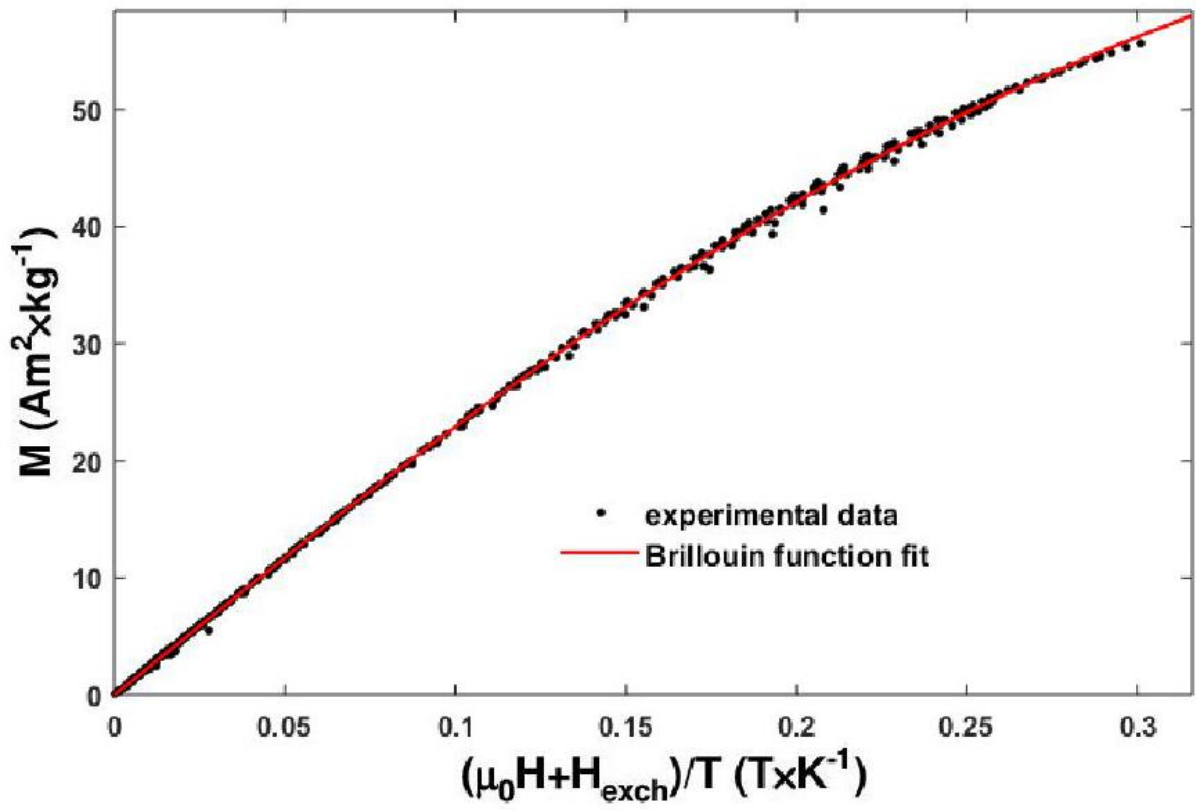
Fig. 7: *M* *vs* $\frac{\mu_0 H + H_{exch}}{T}$ scaling plots fitted using Brillouin function.

Fig. 8: (a) *M vs H* curves (*black symbols*) with the interpolation using the mean-field method (*red lines*). **(b)** *M vs T* curves (*black symbols*) with the interpolation using the Bean- Rodbell model (*red lines*).

Fig. 9: Comparison between $-\Delta S_M$ *vs* *T* under various applied magnetic fields estimated from Maxwell relation (black symbols) and mean field model (red lines).